

# Least-squares spline resampling to a hexagonal lattice

Dimitri Van De Ville<sup>a,\*</sup>, Wilfried Philips<sup>b</sup>, Ignace Lemahieu<sup>a</sup>

<sup>a</sup> *Department of Electronics and Information Systems, Ghent University, Sint-Pietersnieuwstraat 41, B-9000 Gent, Belgium*

<sup>b</sup> *Department of Telecommunications and Information Processing, Ghent University, Sint-Pietersnieuwstraat 41, B-9000 Gent, Belgium*

Received 5 July 2001; received in revised form 22 January 2002; accepted 4 February 2002

---

## Abstract

Resampling is a common operation in digital image processing systems. The standard procedure involves the (conceptual) reconstruction of a continuous image succeeded by sampling on the new lattice sites. When the reconstruction is done by classical interpolation functions, results might be sub-optimal because the information loss is not minimized. In the particular case of subsampling (i.e., resampling to a coarser lattice), aliasing artifacts might arise and produce disturbing moire patterns. This paper first introduces a spline model for different orders, both for orthogonal and hexagonal lattices. Next, an expression for a least-squares approximation is derived which can be applied to convolution-based resampling. Experimental results for a printing application demonstrate the feasibility of the proposed method and are compared against the standard approach. Our technique can be applied to general least-squares resampling between regular lattices. © 2002 Elsevier Science B.V. All rights reserved.

*Keywords:* Bivariate splines; Hexagonal lattice; Linear resampling; Aliasing artifacts; Least-squares resampling; Gravure printing

---

## 1. Introduction

Digital image processing handles images by means of a discrete representation. In particular, the image is sampled at the spatial positions indicated by a regular lattice. The conversion of a discrete image representation on a given lattice to another, is called image resampling. This operation is indispensable for many applications (e.g., desktop-publishing, printing applications, medical applications,...). This paper concentrates on the particular case of resampling to a coarser

grid than the original one. Also, the target lattice is not orthogonal, but hexagonal.

The standard procedure for resampling consists of two conceptual steps: first, the “continuous image” is reconstructed by interpolation; second, this function is resampled on the target lattice [1–4]. Shannon’s sampling theorem assumes images are band-limited, and proposes to choose the interpolation filter to the ideal low-pass filter. However, real-world signals are not band-limited and the image and the interpolation function have a finite support. Due to the slow decay of the ideal interpolation functions (which are sinc-like), it is also quite difficult to approximate them on a finite support. Additionally, ideal interpolators tend to generate the Gibb’s phenomenon, which becomes visually apparent in images as ringing along the edges.

---

\*Corresponding author. Tel.: +32-9-2648917; fax: +32-9-2643594.

*E-mail address:* dimitri.vandeville@rug.ac.be (D. Van De Ville).

<sup>1</sup>Research Assistant of the Fund for Scientific Research – Flanders (Belgium).

Instead of holding on to the band-limited hypothesis, many authors, such as Unser [5–8], set up a family of basis functions based on splines. These splines have a limited size of support, which expands as the order increases. (Ultimately, a spline representation of infinite order approaches the ideal filter.) For example, first-order spline interpolation is better known as “nearest neighbour” interpolation; second-order spline interpolation as bilinear interpolation. Higher orders, such as bicubic spline interpolation yield even smoother results.

The standard approach does not minimize the information loss, in particular when subsampling images. Annoying artifacts due to aliasing (such as moire-patterns) might arise. Applying sufficient lowpass filtering prior to resampling can avoid problems. In practice, e.g., it is a non-trivial task to determine the right amount of filtering prior to resampling. Unser et al. [5,9] derived an algorithm based on the principle of convolution-based least-squares spline approximation. In particular, the samples on the target lattice are chosen such that the mean squared error between the continuous spline representation on the source lattice and a similar one on the target lattice is minimized. This theory was developed for a 1D spline representation, and extended to 2D orthogonal lattices by means of tensor-product splines (i.e., the 2D spline is the product of two 1D splines). Theoretical considerations showed that the approximation power of least-squares approaches is superior to interpolative ones.

This paper discusses the case of resampling to a hexagonal lattice, therefore requiring a spline definition suitable for hexagonal lattices. Common extensions of B-splines to 2D, such as tensor-product splines, cannot be used on this type of lattice. Other spline definitions, such as box splines [10–12], are typically defined on triangular patches and used for geometric modelling (e.g. [13,14]). This paper uses the same underlying principle of box splines (i.e., construction by successive convolutions), but applied to a hexagonal basic shape. This proposition leads to a logical, but non-separable, 2D spline definition suitable for hexagonal lattices. The convolution property will be very useful in the derivation of the reconstruction function corresponding to least-squares resampling from an orthogonal to a hexagonal lattice. We also

derive the approximation order of the hexagonal spline. To demonstrate the feasibility of the proposed approach, we implemented our approach for the practical case of gravure printing, a printing technique which is very susceptible to aliasing artifacts when using standard resampling procedures. The results of this paper can be extended for resampling from any regular lattice to another.

## 2. The 2D spline basis

This section introduces the necessary mathematical background. First we show how to represent a regular 2D lattice. Second, we derive a set of 2D shift-invariant basis functions, both for an orthogonal and a hexagonal lattice.

A continuous 2D function is denoted as  $g(\mathbf{x})$ , where  $\mathbf{x} \in \mathbb{R}^2$ . The  $L_2$ -norm of  $g(\mathbf{x})$  is derived from the inner product

$$\langle g_1, g_2 \rangle = \int g_1(\mathbf{x})g_2(\mathbf{x}) \, d\mathbf{x}, \quad (1)$$

$$\|g\|^2 = \int |g(\mathbf{x})|^2 \, d\mathbf{x}, \quad (2)$$

where the integrations are over the complete plane  $\mathbb{R}^2$ . Analogously, we denote a discrete 2D array as  $c(\mathbf{k})$ , where  $\mathbf{k} \in \mathbb{Z}^2$ . The  $l_2$ -norm of  $c(\mathbf{k})$  is defined as

$$\|c\|_{l_2}^2 = \sum_{\mathbf{k} \in \mathbb{Z}^2} |c(\mathbf{k})|^2. \quad (3)$$

A 2D lattice can be characterized by two linearly independent vectors  $\mathbf{r}_1$  and  $\mathbf{r}_2$ . Each lattice site is represented by the vector [15,16]

$$\begin{aligned} \mathbf{r}_{k_1, k_2} &= k_1 \mathbf{r}_1 + k_2 \mathbf{r}_2, \quad \text{where } k_1, k_2 \in \mathbb{Z} \\ &= [\mathbf{r}_1 | \mathbf{r}_2] \begin{bmatrix} k_1 \\ k_2 \end{bmatrix} \\ &= \mathbf{R}\mathbf{k}, \quad \text{where } \mathbf{k} \in \mathbb{Z}^2. \end{aligned} \quad (4)$$

Thus the lattice is described by the matrix  $\mathbf{R}$ . It is convenient to define an array of impulses on the lattice sites,

$$\delta_{\mathbf{R}}(\mathbf{x}) = \sum_{\mathbf{k}} \delta(\mathbf{x} - \mathbf{R}\mathbf{k}), \quad (5)$$

where  $\delta(\mathbf{x})$  represents a Dirac function.

Related to a lattice is a Voronoi cell, which is defined as the set of all points that are closer to the origin  $\mathbf{0}$  than to any other site of the lattice. The Voronoi cell is represented by its indicator-function  $\chi_{\mathbf{R}}(\mathbf{x})$ :

$$\chi_{\mathbf{R}}(\mathbf{x}) = \begin{cases} 1, & \mathbf{x} \in \text{Voronoi cell,} \\ 1/m, & \mathbf{x} \text{ on edge Voronoi cell,} \\ 0, & \mathbf{x} \notin \text{Voronoi cell,} \end{cases} \quad (6)$$

where  $m$  equals the number of lattice sites to which  $\mathbf{x}$  is equidistant. Note that this function, when periodically copied onto all the lattice sites, covers the complete plane:

$$(\delta_{\mathbf{R}} \star \chi_{\mathbf{R}})(\mathbf{x}) = 1, \quad (7)$$

where the  $\star$ -operator denotes the 2D continuous convolution. It is said that the Voronoi cell tiles the plane. More properties and definitions can be found in [15].

Consider a function, which is sampled on each lattice site of a lattice  $\mathbf{R}$ . Using a shift-invariant 2D generating function  $\phi(\mathbf{x})$ , we define the approximation space  $S$  as follows [17]:

$$S(\phi) = \left\{ s(\mathbf{x}) \mid s(\mathbf{x}) = \sum_{\mathbf{k} \in \mathbb{Z}^2} c(\mathbf{k})\phi(\mathbf{x} - \mathbf{R}\mathbf{k}); c(\mathbf{k}) \in \mathbb{R} \right\}, \quad (8)$$

where the coefficients  $c(\mathbf{k})$  need to be chosen properly. As such, any function  $s(\mathbf{x}) \in S(\phi)$  is characterized by a sequence of coefficients  $c(\mathbf{k})$ . Notice that these coefficients are not necessarily samples  $s(\mathbf{R}\mathbf{k})$  at the lattice points.

In order to have a sensible continuous/discrete model, three conditions are required [17]. First, the coefficients must be square-summable. Second, the family of functions  $\{\phi(\mathbf{x} - \mathbf{k})\}_{\mathbf{k} \in \mathbb{Z}^2}$  should form a Riesz basis of  $S(\phi)$ : there must exist two strictly positive constants  $0 < A$  and  $B < +\infty$  such that

$$A \|c\|_2^2 \leq \left\| \sum_{\mathbf{k}} c(\mathbf{k})\phi(\mathbf{x} - \mathbf{R}\mathbf{k}) \right\|_2^2 \leq B \|c\|_2^2. \quad (9)$$

The Riesz basis ensures that the continuous/discrete model is stable (i.e., a small change of the coefficients produces a small change of the spline representation) and non-ambiguous (i.e., the coefficients are unique for each spline representa-

tion). Finally, and most stringent, the partition of unity condition must be fulfilled:

$$(\delta_{\mathbf{R}} \star \phi)(\mathbf{x}) = 1. \quad (10)$$

### 2.1. A spline basis on the orthogonal lattice

A regular orthogonal lattice is described by the matrix

$$\mathbf{R} = \begin{bmatrix} 1 & 0 \\ 0 & 1 \end{bmatrix}. \quad (11)$$

To form 2D splines on this lattice, we can easily use the tensor-product of two one-dimensional B-splines,

$$\beta^n(\mathbf{x}) = \beta^n(x_1)\beta^n(x_2). \quad (12)$$

The first-order 1D B-spline is defined by

$$\beta^0(x) = \begin{cases} 1, & |x| < \frac{1}{2}, \\ 1/2, & |x| = \frac{1}{2}, \\ 0, & |x| > \frac{1}{2}, \end{cases} \quad (13)$$

which corresponds to a piecewise polynomial of zeroth degree. The term ‘‘order’’ refers to the order of approximation as the sampling density increases [18]. Successive convolutions of  $\beta^0(x)$  with itself define the higher order B-splines,

$$\beta^n(x) = (\beta^{n-1} \star \beta^0)(x), \quad n \geq 1. \quad (14)$$

B-splines are piecewise polynomial functions which are symmetric and of limited support. They are not orthogonal, but they form a Riesz basis and satisfy the partition of unity condition [17]. Many other interesting properties of these functions fall outside the scope of this paper.

### 2.2. A spline basis on the hexagonal lattice

Consider a regular hexagonal lattice described by the matrix

$$\tilde{\mathbf{R}} = \begin{bmatrix} \sqrt{3}/2 & 0 \\ -1/2 & 1 \end{bmatrix}. \quad (15)$$

We define the surface area of the Voronoi cell as  $\Omega = |\det(\tilde{\mathbf{R}})| = \sqrt{3}/2$ . Matrices and functions

related to the hexagonal lattice are denoted by the  $\tilde{\cdot}$ -superscript.

To construct a spline basis on the hexagonal lattice, we are especially interested in preserving the convolution property because it plays an important role in the derivation of the least-squares approximation later on. Therefore, we first define the first-order hexagonal spline as the indicator function of the Voronoi cell,

$$\tilde{\beta}^0(\mathbf{x}) = \chi_{\tilde{R}}(\mathbf{x}). \tag{16}$$

Note that this spline is normalized to the surface area of the basic cell:  $\int \tilde{\beta}^0 \, d\mathbf{x} = \Omega$ . By convolving this function with itself repeatedly, we construct

hexagonal splines of higher orders,

$$\tilde{\beta}^n(\mathbf{x}) = \frac{(\tilde{\beta}^0 \star \tilde{\beta}^{n-1})(\mathbf{x})}{\Omega}, \quad n \geq 1. \tag{17}$$

Fig. 1 shows the hexagonal splines from first to fourth order. The successive convolutions imply that the splines become smoother as the order increases. The above approach also ensures properties such as positivity and convexity [19]. The primary focus of this paper is not the analytic form of these splines, but Appendix A derives an analytic form for the second-order hexagonal spline and Appendix B shows a useful approximation for higher splines. Finally, Appendix C shows

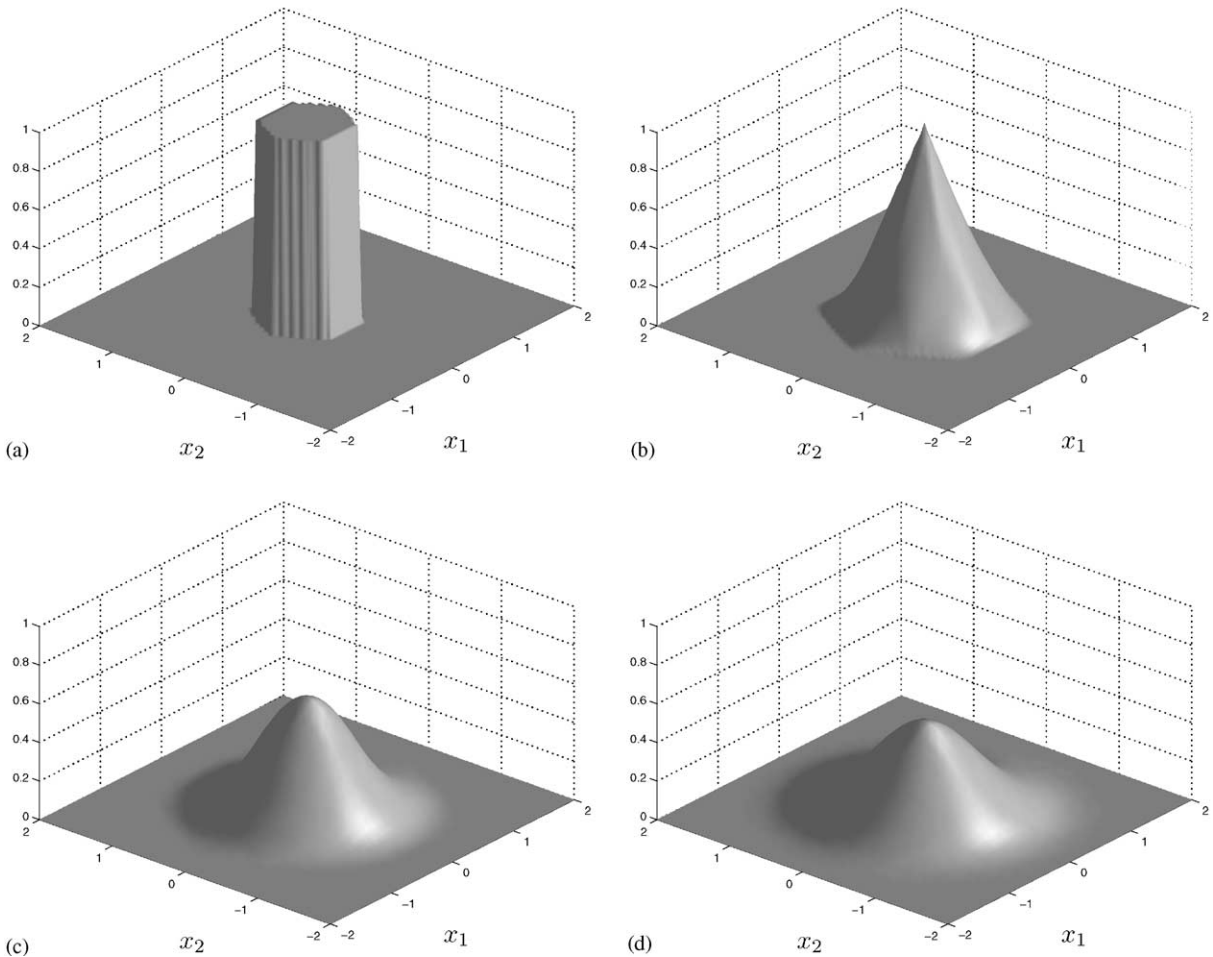


Fig. 1. Splines derived on a hexagonal lattice: (a) first order, (b) second order, (c) third order, (d) fourth order.

that the hexagonal spline order corresponds to the approximation order.

Without a formal proof that the hexagonal splines form a Riesz basis, we indicate that this requirement is satisfied. First, it is easy to show that Eq. (9) holds for the first-order hexagonal spline with  $A = B = \Omega$ . For higher orders, the upper limit remains the same. If we take into account the proper normalization and positivity of  $\tilde{\beta}^n(\mathbf{x})$ , we can conclude that a lower limit must exist for  $n < +\infty$ .

Using the recursive construction of Eq. (17) and the basic property of Eq. (16), it is very easy to show that the splines obtained in this way also satisfy the partition of unity, i.e., they meet the requirement

$$(\delta_{\tilde{\mathbf{R}}} \star \tilde{\beta}^n)(\mathbf{x}) = 1. \tag{18}$$

### 2.3. The spline transform

For both regular lattices considered in this paper, we now have a suitable spline definition. Our spline signal representation can be described as follows:

$$g^n(\mathbf{x}) = \sum_k c(\mathbf{k})\beta^n(\mathbf{x} - \mathbf{Rk}), \tag{19}$$

according to Eq. (8). Note that this and following equations of this section apply also to the hexagonal lattice. Consider now a function  $g(\mathbf{x})$ , which is represented in the spline space  $S^n$  as  $g^n(\mathbf{x})$ , and constructed as the weighted sum of shifted splines. As such,  $g^n(\mathbf{x})$  is uniquely characterized by its spline coefficients  $c(\mathbf{k})$ . To obtain the spline coefficients, we need to introduce the “sampled spline”,

$$b^n(\mathbf{x}) = \beta^n(\mathbf{x})\delta_{\mathbf{R}}(\mathbf{x}). \tag{20}$$

Let us now consider the spline representation at its lattice site, where we require the spline to *interpolate* the original sample values:  $g(\mathbf{x}) = g^n(\mathbf{x})$  at  $\mathbf{x} = \mathbf{Rk}$ . We make use of Eq. (19) to write

$$\begin{aligned} \delta_{\mathbf{R}}(\mathbf{x})g(\mathbf{x}) &= \delta_{\mathbf{R}}g^n(\mathbf{x}) \\ &= \delta_{\mathbf{R}}(\mathbf{x}) \left( \left[ \sum_k \delta(\mathbf{x} - \mathbf{Rk})c(\mathbf{k}) \right] \star \beta^n \right)(\mathbf{x}), \end{aligned} \tag{21}$$

such that

$$c(\mathbf{k}) = ((b^n)^{-1} \star g)(\mathbf{Rk}). \tag{22}$$

Substituting this into Eq. (19) enables us to write the “cardinal spline form”,

$$g^n(\mathbf{x}) = \sum_k (((b^n)^{-1} \star \beta^n)(\mathbf{x}))g(\mathbf{Rk}). \tag{23}$$

Solving Eq. (22) is referred to as the direct spline transform. The computation of the inverse filter  $(b^n)^{-1}$  will be covered in Section 4. Note that for  $n = 0, 1$ , the inverse filters  $(b^0)^{-1}$  and  $(b^1)^{-1}$  are trivial, i.e., the spline coefficients  $c(\mathbf{k})$  are identical to  $g(\mathbf{Rk})$ .

### 3. The 2D least-squares approximation

In this section, we formally derive the least-squares approximation for a resampling procedure from the signal space  $S^n$  to  $\tilde{S}^n$ . Consider two spline representations, one on the source lattice and one on the target lattice,

$$\begin{aligned} g^n(\mathbf{x}) &= \sum_k c(\mathbf{k})\beta^n(\mathbf{x} - \mathbf{Rk}), \\ \tilde{g}^n(\mathbf{x}) &= \sum_k \tilde{c}(\mathbf{k})\tilde{\beta}^n(\mathbf{x} - \tilde{\mathbf{R}}\mathbf{k}). \end{aligned}$$

We want to obtain those new sample values  $\tilde{g}^n(\tilde{\mathbf{R}}\mathbf{k})$  such that the squared error between  $g^n(\mathbf{x})$  and  $\tilde{g}^n(\mathbf{x})$  is minimized. For that purpose, we derive a proper reconstruction function  $\Phi^n(\mathbf{x})$  which obtains

$$\begin{aligned} \tilde{g}^n(\tilde{\mathbf{R}}\mathbf{k}) &= s(\tilde{\mathbf{R}}\mathbf{k}), \\ \text{with } s(\mathbf{x}) &= \sum_k \Phi^n(\mathbf{x} - \mathbf{Rk})g(\mathbf{Rk}). \end{aligned} \tag{24}$$

Fig. 2 illustrates the principle of least-squares resampling.

The minimum  $L_2$ -norm approximation of a function  $g(\mathbf{x})$  in the signal space  $\tilde{S}^n$  can be found by projection on  $\tilde{S}^n$ . As such, the error  $g(\mathbf{x}) - \tilde{g}^n(\mathbf{x})$  is orthogonal to  $\tilde{S}^n$ . Since the original function  $g$  is only known at the lattice sites  $\mathbf{Rk}$ , we assume  $g$  can be adequately modelled by its spline representation  $g^n$ , part of  $S^n$ . This enables us to write

$$\langle g^n(\mathbf{x}) - \tilde{g}^n(\mathbf{x}), \tilde{\beta}^n(\mathbf{x} - \tilde{\mathbf{R}}\mathbf{k}) \rangle = 0, \tag{25}$$

where  $g^n(\mathbf{x})$  and  $\tilde{g}^n(\mathbf{x})$  are the spline representations, respectively, on the orthogonal and

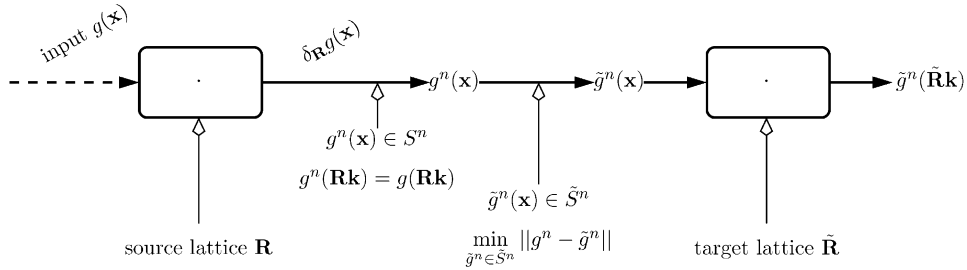


Fig. 2. Least-squares resampling computes the new sample values  $\tilde{g}^n(\tilde{\mathbf{R}}\mathbf{k})$  on the target lattice such that the squared error  $\|g^n - \tilde{g}^n\|^2$  between the spline representation on the source lattice and the target lattice is minimized.

hexagonal lattice. Using Eq. (19), we can rewrite the expression as

$$\begin{aligned} &\langle g^n(\mathbf{x}), \tilde{\beta}^n(\mathbf{x} - \tilde{\mathbf{R}}\mathbf{k}) \rangle \\ &= \left\langle \sum_k \tilde{c}(\mathbf{k}) \tilde{\beta}^n(\mathbf{x} - \tilde{\mathbf{R}}\mathbf{k}), \tilde{\beta}^n(\mathbf{x} - \tilde{\mathbf{R}}\mathbf{k}) \right\rangle \\ &= \sum_k \tilde{c}(\mathbf{k}) \langle \tilde{\beta}^n(\mathbf{x} - \tilde{\mathbf{R}}\mathbf{k}), \tilde{\beta}^n(\mathbf{x} - \tilde{\mathbf{R}}\mathbf{k}) \rangle, \end{aligned} \quad (26)$$

where  $\tilde{c}(\mathbf{k})$  are the spline coefficients on the hexagonal lattice. We now use the founding property of the hexagonal splines  $(\tilde{\beta}^n \star \tilde{\beta}^n)(\mathbf{x})/\Omega = \tilde{\beta}^{2n+1}(\mathbf{x})$ .

$$\begin{aligned} &(g^n \star \tilde{\beta}^n(\mathbf{x})) \\ &= \Omega \left( \left[ \sum_k \delta(\mathbf{x} - \tilde{\mathbf{R}}\mathbf{k}) \tilde{c}(\mathbf{k}) \right] \star \tilde{\beta}^{2n+1} \right)(\mathbf{x}). \end{aligned} \quad (27)$$

The solution of Eq. (26) can be written as

$$\tilde{c}(\mathbf{k}) = \frac{g^n \star \tilde{\beta}^n \star (\tilde{b}^{2n+1})^{-1}}{\Omega}(\mathbf{R}\mathbf{k}). \quad (28)$$

This enables us to write the least-squares reconstruction function for resampling from the lattice  $\mathbf{R}$  to  $\tilde{\mathbf{R}}$  as

$$\begin{aligned} \Phi^n(\mathbf{x}) = & \left( \underbrace{(b^n)^{-1} \star \beta^n}_1 \star \underbrace{\tilde{\beta}^n \star (\tilde{b}^{2n+1})^{-1}}_2 \star \underbrace{\tilde{b}^n}_3 \right)(\mathbf{x})/\Omega, \end{aligned} \quad (29)$$

where the underbraced expressions indicate:

- (1) the direct spline transform to compute the spline coefficients on the source lattice;

- (2) the least-squares approximation filter;
- (3) the final convolution to reconstruct the values at the target lattice sites in the signal space  $\tilde{S}^n$  using the new spline coefficients.

Once the reconstruction function  $\Phi^n(\mathbf{x})$  is known, it can be used by Eq. (24) to compute directly the least-squares sample values on the target lattice.

#### 4. Computational issues

The direct spline transform and the least-squares approximation filter require the computation of inverse filters. The  $\mathcal{L}$ -transform representation is well suited to represent these filters. The 1D  $\mathcal{L}$ -transform is given by

$$B(z) = \sum_{k \in \mathbb{Z}} \beta(k) z^k. \quad (30)$$

Similarly, we define the 2D  $\mathcal{L}$ -transform, associated to a given lattice  $\mathbf{R}$ , as

$$B(z_1, z_2) = \sum_k \beta(\mathbf{R}\mathbf{k}) z_1^{k_1} z_2^{k_2}, \quad (31)$$

The 1D direct B-spline transform of Eq. (22) has been studied extensively (and therefore also the 2D orthogonal transform due to separability). Many publications (e.g. [20]) are devoted to efficient techniques for inverting the matrix corresponding to the set of linear equations of Eq. (22). A fast inversion scheme by means of two recursive filters is described in [6,21].

Table 1 shows the  $\mathcal{L}$ -transform of the spline filters. Starting from  $n = 2$ , the inverse hexagonal spline filters are complicated and also require an infinite support. Due to non-separability, matrix

Table 1  
 $\mathcal{L}$ -transforms of the basic spline kernels for the 1D B-splines and the 2D hexagonal splines

$n$	B-spline filter	Hexagonal spline filter
0	$B^0(z) = 1$	$B^0(z_1, z_2) = 1$
1	$B^1(z) = 1$	$B^1(z_1, z_2) = 1$
2	$B^2(z) = \frac{6}{8} + \frac{1}{8}(z + z^{-1})$	$B^2(z_1, z_2) = \frac{42}{72} + \frac{5}{72}(z_1 + z_2 + z_1^{-1} + z_2^{-1} + z_1 z_2 + z_1^{-1} z_2^{-1})$
3	$B^3(z) = \frac{4}{6} + \frac{1}{6}(z + z^{-1})$	$B^3(z_1, z_2) = \frac{37}{81} + \frac{29}{324}(z_1 + z_2 + z_1^{-1} + z_2^{-1} + z_1 z_2 + z_1^{-1} z_2^{-1}) + \frac{1}{972}(z_1^{-1} z_2 + z_1 z_2^{-1} + z_1 z_2^2 + z_1^{-1} z_2^{-2} + z_1^2 z_2^2 + z_1^{-2} z_2^{-2})$

inversion requires much memory. Also, an implementation using recursive filters based on the decomposition of the inverse 2D hexagonal spline filter is difficult because factorization is not trivial (e.g., of  $1/B^3(z_1, z_2)$ ). Based on the observation that the cardinal splines have a fast decay, we will approximate the least-squares reconstruction function on a limited support. We now present the results for different  $n$  more closely.

In the case of  $n = 0$ , the reconstruction function of Eq. (29) becomes

$$\Phi^0(\mathbf{x}) = (\beta^0 \star \tilde{\beta}^0)(\mathbf{x})/\Omega. \tag{32}$$

No inverse filters are needed. Also, the support is limited. This case is sometimes referred to as “surface projection”, which is illustrated in Fig. 3. In order to obtain a new sample value for the central lattice site  $\tilde{\mathbf{p}}_0$ , neighbouring samples on the source lattice are taken and weighted by the relative overlap of their cell surface area. Note the difference with first-order interpolation, which would simply assign the value of the nearest source cell (i.e.,  $\mathbf{p}_2$ ) to the origin (Fig. 4).

For the second-order least-squares approximation, the reconstruction function is given by

$$\Phi^1(\mathbf{x}) = (\beta^1 \star (\tilde{b}^3)^{-1} \star \tilde{\beta}^1(\mathbf{x}))/\Omega. \tag{33}$$

The presence of the inverse filter  $(\tilde{b}^3)^{-1}$  implicates that the theoretical support of  $\Phi^1(\mathbf{x})$  is the whole plane. However, the fast decay shows that an approximation on a limited support is appropriate. In particular, the filter  $\tilde{\beta}^1 \star (\tilde{b}^3)^{-1}$  is computed

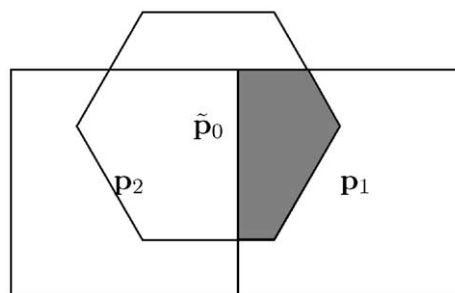


Fig. 3. The first-order least-squares approximation corresponds to “surface projection”. For example, the contribution of the sample value at  $\mathbf{p}_1$  to the resampled value at  $\tilde{\mathbf{p}}_0$  on the target lattice is proportional to the shared surface area (indicated in gray).

by solving the following equation for  $f(\mathbf{x})$ :

$$\tilde{\beta}^1(\mathbf{x}) = (\tilde{b}^3 \star f)(\mathbf{x}). \tag{34}$$

An iterative procedure updates an estimate  $f(\mathbf{x})$  in each iteration [22],

$$f_0(\mathbf{x}) = \lambda \tilde{\beta}^1(\mathbf{x}),$$

$$f_{k+1}(\mathbf{x}) = f_k(\mathbf{x}) + \lambda(\tilde{\beta}^1(\mathbf{x} - f_k \star \tilde{b}^3(\mathbf{x})).$$

Note that the convolution at the righthand side of the iteration is very simple to evaluate because the hexagonal spline  $\tilde{\beta}^3(\mathbf{x})$  is of limited support,

$$f_k \star \tilde{b}^3(\mathbf{x}) = \sum_k \tilde{\beta}^3(\mathbf{Rk})f_k(\mathbf{x} - \mathbf{Rk}). \tag{35}$$

Here  $\lambda$  is a parameter which is positive and can be used to control the convergence behavior of the

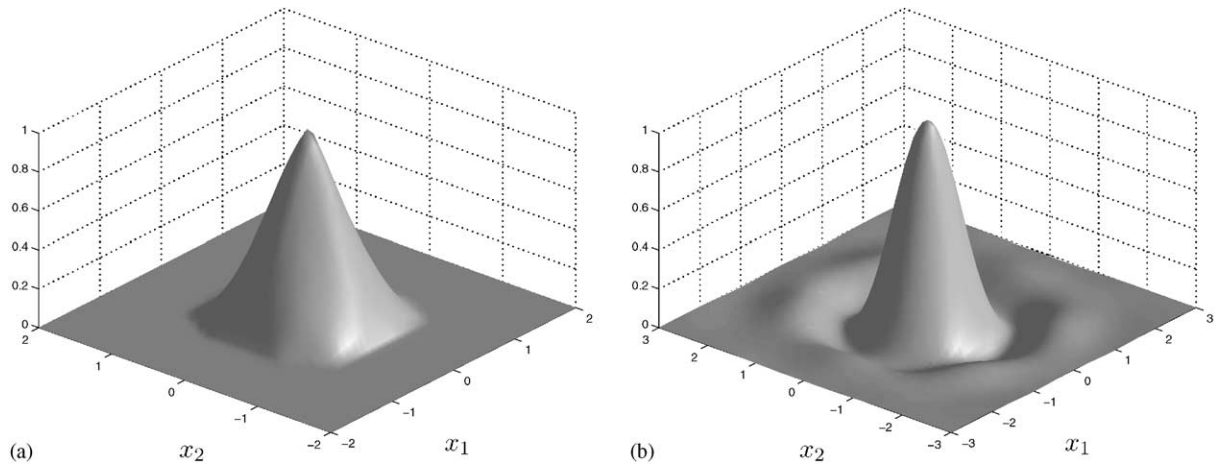


Fig. 4. Least-squares reconstruction function: (a) “surface projection”  $\Phi^0(x)$ , (b)  $\Phi^1(x)$ .

iterative procedure. As a matter of fact, convergence is guaranteed if  $\lambda$  satisfies

$$|1 - \lambda B^3(e^{-j2\pi f_1}, e^{-j2\pi f_2})| < 1, \quad \forall f_1, f_2 \in \mathbb{R}, \quad (36)$$

where  $B^3(z_1, z_2)$  is the  $\mathcal{Z}$ -transform of the filter  $\tilde{b}^3$ . Therefore,  $B^3(e^{-j2\pi f_1}, e^{-j2\pi f_2})$  is the frequency response of the filter and the vector  $\mathbf{f} = (f_1, f_2)$  points to a frequency component  $\hat{\mathbf{R}}\mathbf{f}$ , where  $\hat{\mathbf{R}}$  is the dual lattice [16,23] of  $\mathbf{R}$ , i.e.  $(\mathbf{R}^{-1})^T$ . Note that due to symmetry, the frequency response of the filters of Table 1 are real-valued. The normalization of the splines also implies that

$$\max(B^3(e^{-j2\pi f_1}, e^{-j2\pi f_2})) = 1. \quad (37)$$

To converge,  $\min(B^3(e^{-j2\pi f_1}, e^{-j2\pi f_2}))$  must be positive. This requirement can be easily verified.

Higher orders can be computed similarly, but require the computation of two inverse filters (e.g., we can compute separately the inverse filters of parts 1 and 2 in Eq. (29)). Note that it is also possible to use different orders on the source and the target lattice.

## 5. Results

To demonstrate the feasibility of the proposed approach, we consider the practical setting on a more general hexagonal target lattice, i.e., the case

of gravure printing. Like most printing processes, gravure printing requires the use of halftoning techniques to create the illusion of continuous-tone images. Gravure printing uses classical halftoning, i.e., a diamond engraves little notches into the printing plate that correspond to dots of varying sizes according to the notch's depth. These dots are placed upon a regular hexagonal lattice, and thus a resampling procedure is required to obtain the sample values on this hexagonal lattice. Typical gravure printing is well suited for huge volumes, but uses rather a coarse halftone lattice. In our particular case, the source lattice is an orthogonal  $300 \times 300$  dpi normalized lattice (i.e. Eq. (11)). The target lattice is given by

$$\tilde{\mathbf{R}} = \begin{bmatrix} 1.42 & 0 \\ -1.18 & 2.36 \end{bmatrix}. \quad (38)$$

Fig. 5 shows the Voronoi cells of the source lattice and the target lattice. The low resolution of the target lattice renders gravure printing very susceptible to moiré formation: interaction of the periodic screen lattice with the contents of the original image may lead to sampling-moiré due to aliasing [24]. In practice, preparing the printing plates is a costly operation.

We compare our technique against classical interpolation techniques. The acronyms  $IRn$  and  $LSRn$  refer to respectively interpolative resampling

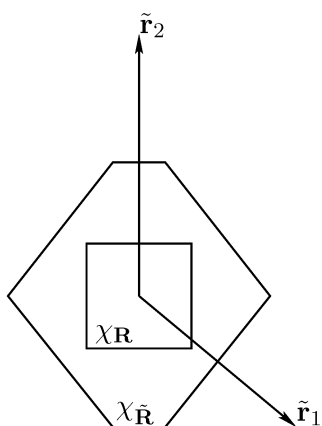


Fig. 5. The Voronoi cell of the source lattice  $\chi_R$  and the gravure printing lattice  $\chi_{\tilde{R}}$ .

and the proposed least-squares resampling, where  $n + 1$  denotes the order of the spline.

The least-squares resampling reconstruction function is numerically approximated on a size of support of  $8 \times 8$ , which results in a ratio of 1% of the largest values inside and outside this support.<sup>2</sup> Figs. 8(a) and (b) show the first-order and second-order resampling filters. Their corresponding amplitude frequency response is depicted in Figs. 8(c) and (d). While the “surface projection” frequency response is still rather low-pass, the second-order response “resembles” already the indicator function of the natural Nyquist area (i.e., the Voronoi cell of the dual target lattice [25,26]). Note the difference with a least-squares approximation for digital filter design, where the squared error between the magnitude frequency response and a prescribed frequency response is minimized [27].

Fig. 6 shows the well-known test image “barbara”, which contains high frequency features such as the stripes in the clothes. Fig. 7 shows another test image “text” to investigate the effect on sharp edges.

Fig. 9 shows results after resampling the “barbara” test image ( $512 \times 512$ ). The halftoning process of the gravure printing was simulated



Fig. 6. Original test image “barbara”.

## Text: An example

Fig. 7. Original test image “text”.

and the results need to be observed at a double normal viewing distance (about 60 cm). Note the blockiness and disturbing moire patterns of the “nearest neighbour” interpolation (IR0). The result using bilinear interpolation (IR1) has less manifest moire patterns but is slightly more blurred. The “surface projection” (LSR0) already suppresses the aliasing artifacts well, but gives too much blurring. Finally, first-order least-squares resampling (LSR1) is clearly the best resampling technique: good moire-suppression, and sharp edges (e.g., the face and the scarf). Fig. 10 shows the results for  $n = 3$ . The interpolative result (IR3) becomes sharper again, but also the moire patterns are more apparent. The difference between LSR3 and LSR1 is almost unnoticeable.

Fig. 11 shows the results after resampling the test image “text” (again, the viewing distance should be doubled). Clearly, IR0 produces jaggy and blocky edges. Both IR1 and LSR1 have smoother results. Finally, LSR1 gives natural

<sup>2</sup>This can be verified by computing the reconstruction function for a larger support first.

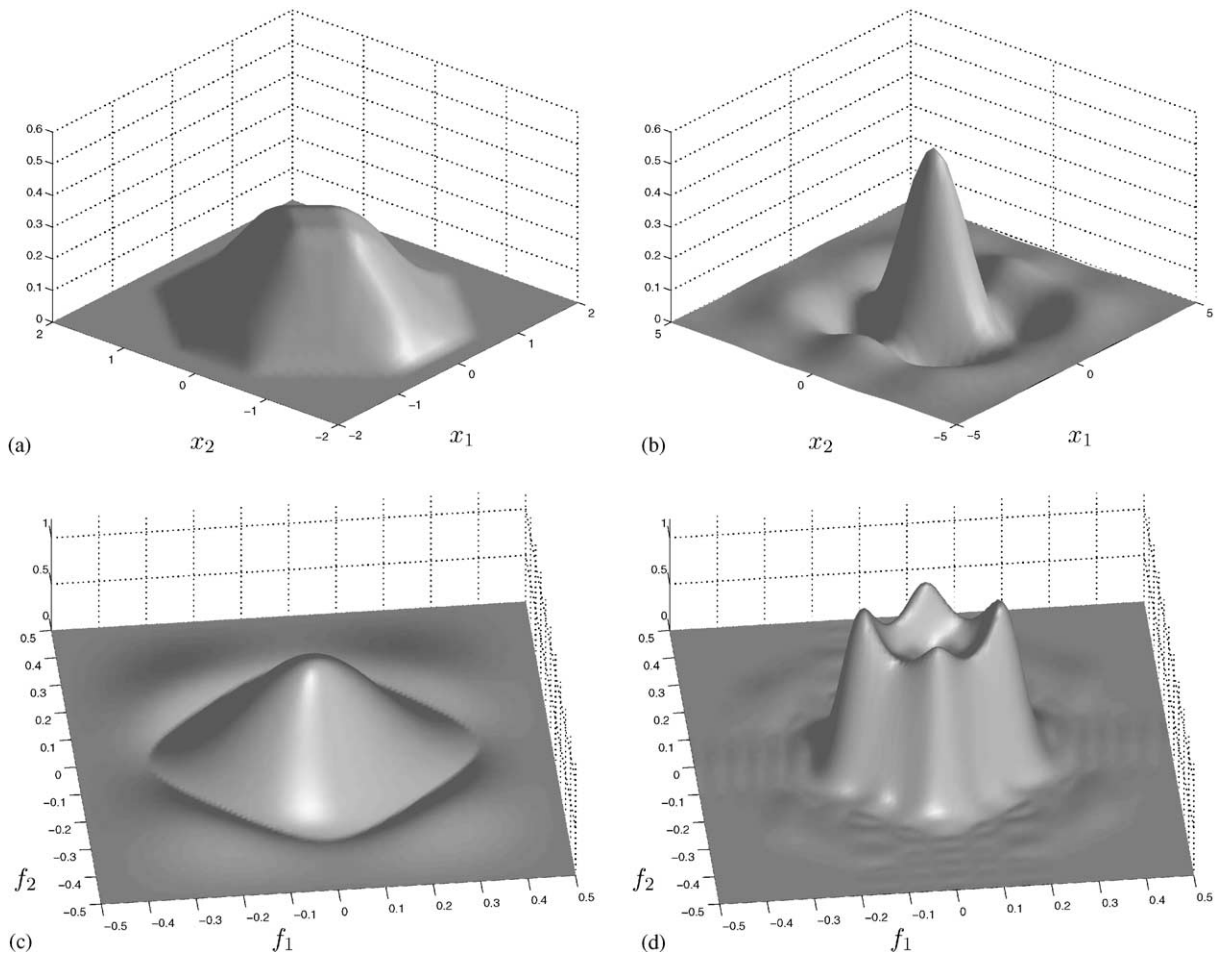


Fig. 8. Least-squares reconstruction function for the gravure printing case study. (a) “Surface projection”  $\Phi^0(x)$ . (b)  $\Phi^1(x)$ . Frequency amplitude response of the least-squares reconstruction function of (c)  $\Phi^0(x)$  and (d)  $\Phi^1(x)$ , respectively.

and sharp edges, but already introduces some ringing (although acceptable at normal viewing distance). These artifacts increase with larger order.

A final interesting test image is “zoneplate”, shown in Fig. 12. A “zoneplate” is a synthetic test image ( $256 \times 256$ ) with increasing frequencies in both horizontal and vertical directions. The top left corner corresponds to the zero spatial frequency, the right and bottom border correspond to the frequencies at the border of the Nyquist area. Clearly, the results using interpolative resampling in Figs. 13(a)–(c) do not suppress frequency components too high for the gravure

lattice, giving rise to disturbing moire artifacts. The results in Figs. 13(d)–(f) use the proposed least-squares approach and are well adapted to the gravure lattice. Notice the rather small difference between LSR1 and LSR3.

## 6. Conclusion

The standard procedure to resample images is to reconstruct a continuous image followed by sampling on the new lattice sites. Typical interpolation functions are not adapted to the characteristics of the target lattice. This paper explains



Fig. 9. Results after resampling the test image “barbara” to the gravure lattice: (a) IR0, (b) IR1, (c) LSR0, (d) LSR1.

a least-squares approach which minimizes the information loss when resampling to a hexagonal lattice. In particular, resampling to a coarser lattice without proper precautions can introduce annoying moiré patterns due to aliasing.

The article presents a spline basis suited for a hexagonal lattice. Splines of different orders are

constructed by successive convolutions, which ensures useful properties such as positivity and convexity. The convolution property is important to derive an expression for the least-squares based reconstruction function. The practical importance of this technique is shown by a printing example. The results show that the quality of least-squares

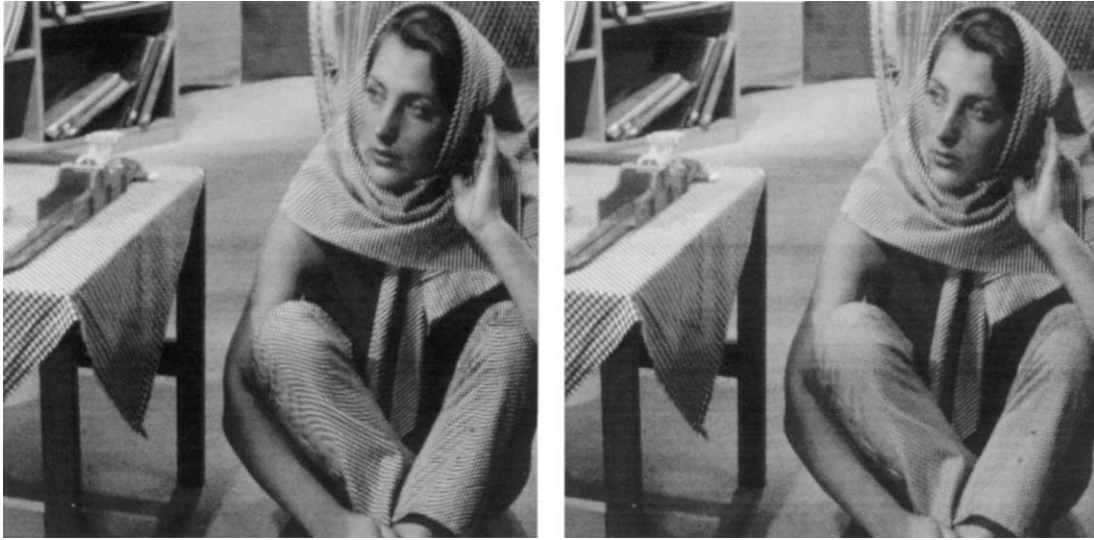


Fig. 10. Results after resampling the test image “barbara” to the gravure lattice: (a) IR3, (b) LSR3.

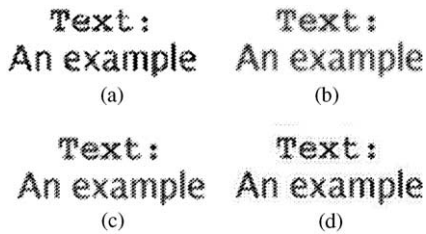


Fig. 11. Results after resampling the test image “text” to the gravure lattice: (a) IR0, (b) IR1, (c) LSR0, (d) LSR1.

resampling is better than interpolative resampling, even for a low order. The approach can be extended for resampling between regular lattices.

**Appendix A. Second-order hexagonal spline**

This appendix shows the analytical solution of the second-order hexagonal spline corresponding to the regular hexagonal lattice of Eq.(15). Fig. 14(a) shows the central Voronoi cell and its neighbour at  $(\sqrt{3}/2, 1/2)$ . The first-order spline is given by the (normalized) convolution of the Voronoi cell with itself. Therefore, the outer

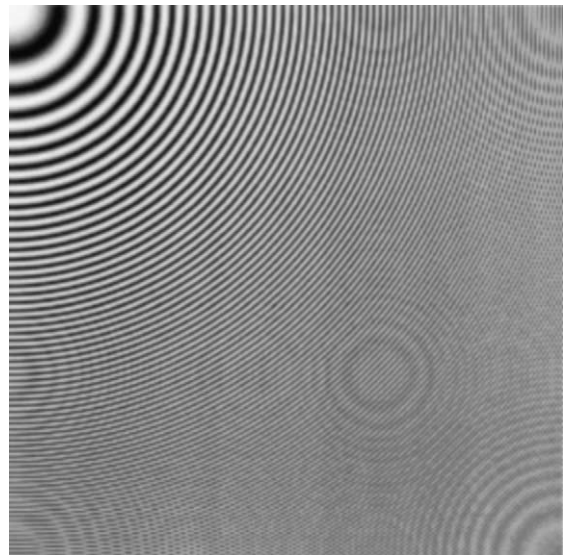


Fig. 12. Original test image “zoneplate”.

dashed line is the support of the spline. If we “shift” the adjacent Voronoi cell along the inner dashed lines, the increments of shared surface area with the central cell vary linearly with the shifted distance. The value at the origin is 1, while the

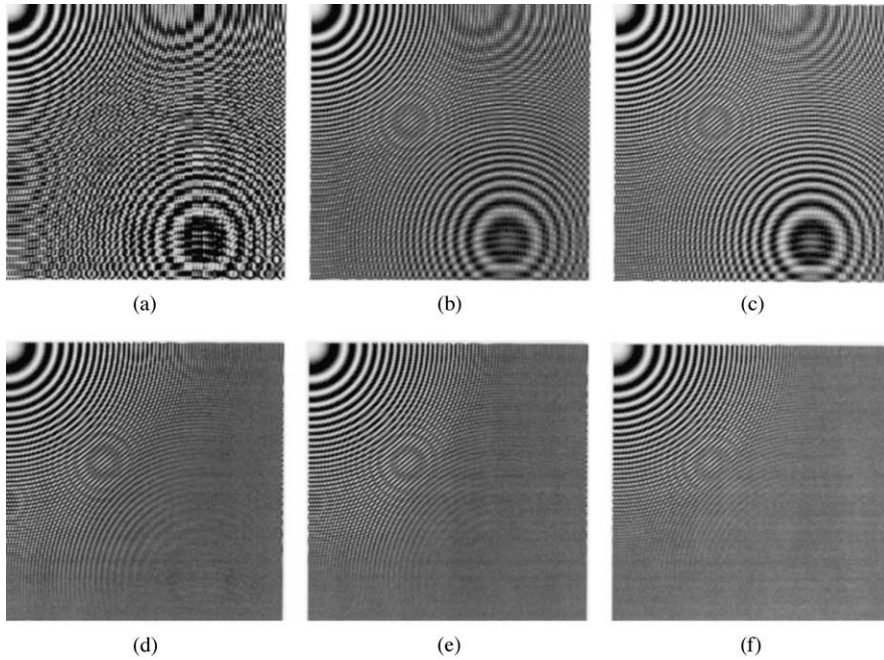


Fig. 13. Results after resampling the “zoneplate” test image to gravure lattice: (a) IR0, (b) IR1, (c) IR3, (d) LSR0, (e) LSR1, (f) LSR3.

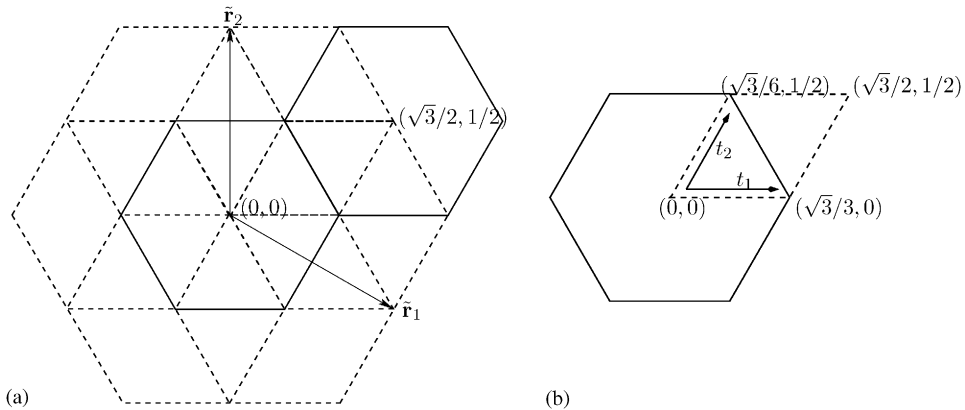


Fig. 14. (a) The second-order hexagonal spline can be divided in regular rhombs. (b) The surface inside each rhomb can be described by using two parameter variables  $(t_1, t_2)$ .

values at the corners of the central cell are  $1/3$ . Inside the rhombs indicated by dashed lines, there is a “linear patch”. For example, Fig. 14(b) shows the rhomb  $(0, 0)$ ,  $(\sqrt{3}/3, 0)$ ,  $(\sqrt{3}/2, 1/2)$ ,  $(\sqrt{3}/6, 1/2)$ . The surface inside a rhomb can be easily described by two parameter variables  $t_1$  and  $t_2$  (which can be obtained using an isoparametric transformation). If we define the parameters  $t_1$  and

$t_2$ , we address every location in the rhomb as  $[0, 1] \times [0, 1]$ . The value inside the rhomb is given by

$$f(t_1, t_2) = (1 - t_1)(1 - t_2) + \frac{t_1(1 - t_2)}{3} + \frac{(1 - t_1)t_2}{3}. \tag{A.1}$$

The analytical form of the third-order hexagonal spline is much more cumbersome and we will not engage into this.

### Appendix B. Approximating the higher order hexagonal splines

Using the bivariate central limit theorem (CLT), it is fairly easy to show that the hexagonal spline converges to a bivariate normal distribution. In particular, if we consider the first-order hexagonal spline  $\tilde{\beta}^0(\mathbf{x})$  as a probability density function (normalized to  $\Omega$ ), then the mean vector  $\mu$  and covariance matrix  $\Sigma$  are given respectively by

$$\mu = \begin{bmatrix} 0 \\ 0 \end{bmatrix}, \quad (\text{B.1})$$

$$\Sigma = \begin{bmatrix} \frac{5\sqrt{3}}{144} & 0 \\ 0 & \frac{5\sqrt{3}}{144} \end{bmatrix}. \quad (\text{B.2})$$

As a consequence, the limit

$$\tilde{\beta}^n(\mathbf{x}) \rightarrow \Omega N_2(\mu, (n+1)\Sigma/\Omega) \quad (\text{B.3})$$

applies. The probability density function of a bivariate normal distribution  $N_2(\mu, \Sigma)$  is given by

$$\frac{1}{2\pi\sqrt{|\det(\Sigma)|}} \exp(-(\mathbf{x} - \mu)^T \Sigma^{-1}(\mathbf{x} - \mu)). \quad (\text{B.4})$$

For the fourth-order hexagonal spline of Fig. 1(d), the relative mean squared error between the real spline and the approximation is only 0.43%.

### Appendix C. Approximation order of the hexagonal spline basis

Let us consider an arbitrary function  $g(\mathbf{x})$ , which is only known at its sampling sites  $g(\tilde{\mathbf{R}}_h \mathbf{k})$  on a hexagonal lattice. The lattice  $\tilde{\mathbf{R}}_h$  stands for  $\tilde{\mathbf{R}}_h = h\tilde{\mathbf{R}}$ , where  $h$  is a positive real number. The representation of this function in our hexagonal spline space is given by

$$g^n(\mathbf{x}) = \sum_{\mathbf{k}} c(\mathbf{k}) \tilde{\beta}^n(\mathbf{x} - \tilde{\mathbf{R}}_h \mathbf{k}). \quad (\text{C.1})$$

As we make  $h$  smaller, we obtain a denser lattice and could reasonably expect  $g^n(\mathbf{x})$  to approach

$g(\mathbf{x})$ . The approximation error in the Fourier domain is given by [28]

$$\eta^2(h) = \frac{1}{2\pi} \int |\hat{g}^n(\mathbf{f})|^2 E_{\text{int}}(\mathbf{f}h) d\mathbf{f}, \quad (\text{C.2})$$

where  $E_{\text{int}}(\mathbf{f})$  is called the interpolation error kernel depending on the basis function only, and  $\hat{g}^n(\mathbf{f})$  is the Fourier transform of  $g^n(\mathbf{f})$ . It is straightforward to extend the kernel of [28] for a general regular lattice,

$$E_{\text{int}}(\mathbf{f}) = \frac{|\sum_{\mathbf{k} \in \mathbf{0}} \hat{\beta}^n(\mathbf{f} + \hat{\mathbf{R}}\mathbf{k})|^2 + \sum_{\mathbf{k} \in \mathbf{0}} |\hat{\beta}^n(\mathbf{f} + \hat{\mathbf{R}}\mathbf{k})|^2}{|\sum_{\mathbf{k}} \hat{\beta}^n(\mathbf{f} + \hat{\mathbf{R}}\mathbf{k})|^2},$$

where  $\hat{\mathbf{R}}$  is the reciprocal lattice of  $\tilde{\mathbf{R}}$ . To compute this kernel, we can use the analytical knowledge of the Fourier transform of the hexagonal spline basis functions. In particular, the Fourier transformed first-order hexagonal spline  $\hat{\beta}^0(\mathbf{x})$  is given by [29]

$$\begin{aligned} \hat{\beta}^0(\mathbf{f}) &= \frac{1}{\pi^2 f_1} \left( \frac{\cos(\pi f_1/\sqrt{3} + \pi f_2) - \cos(2\pi f_2/\sqrt{3})}{f_1 - \sqrt{3}f_2} \right. \\ &\quad \left. + \frac{\cos(-\pi f_1/\sqrt{3} + \pi f_2) - \cos(2\pi f_2/\sqrt{3})}{f_1 + \sqrt{3}f_2} \right). \end{aligned}$$

Due to the convolution theorem, the Fourier transform of the higher order splines is given by

$$\hat{\beta}^n(\mathbf{f}) = (\hat{\beta}^0(\mathbf{f}))^{n+1} / \Omega^n. \quad (\text{C.3})$$

Fig. 15 shows the interpolation error kernel  $E_{\text{int}}$  for the first to fourth order hexagonal spline. Low frequency components give rise to a low approximation error. Frequency components too high for the lattice contribute twice to the approximation error: once because they cannot be reproduced in  $\tilde{S}^n$ , and once because they give rise to aliasing. For a higher order, a clear boundary arises at the border of the Nyquist area [26].

Since decreasing  $h$  in Eq. (C.2) makes the argument of  $E_{\text{int}}$  smaller, the error kernel must vanish at the origin. The approximation order relates to the vanishing rate of the error, i.e.,  $\eta(h) \propto h^L$ . To determine the approximation order  $L$ , we can also verify the equivalent first Strang-Fix condition [18], i.e.,  $\hat{\beta}(\mathbf{0}) = 1$  and all the partial derivatives  $\partial^2/\partial f_1^{m_1} \partial f_2^{m_2}$  of  $\hat{\beta}(\hat{\mathbf{R}}\mathbf{k})$  where

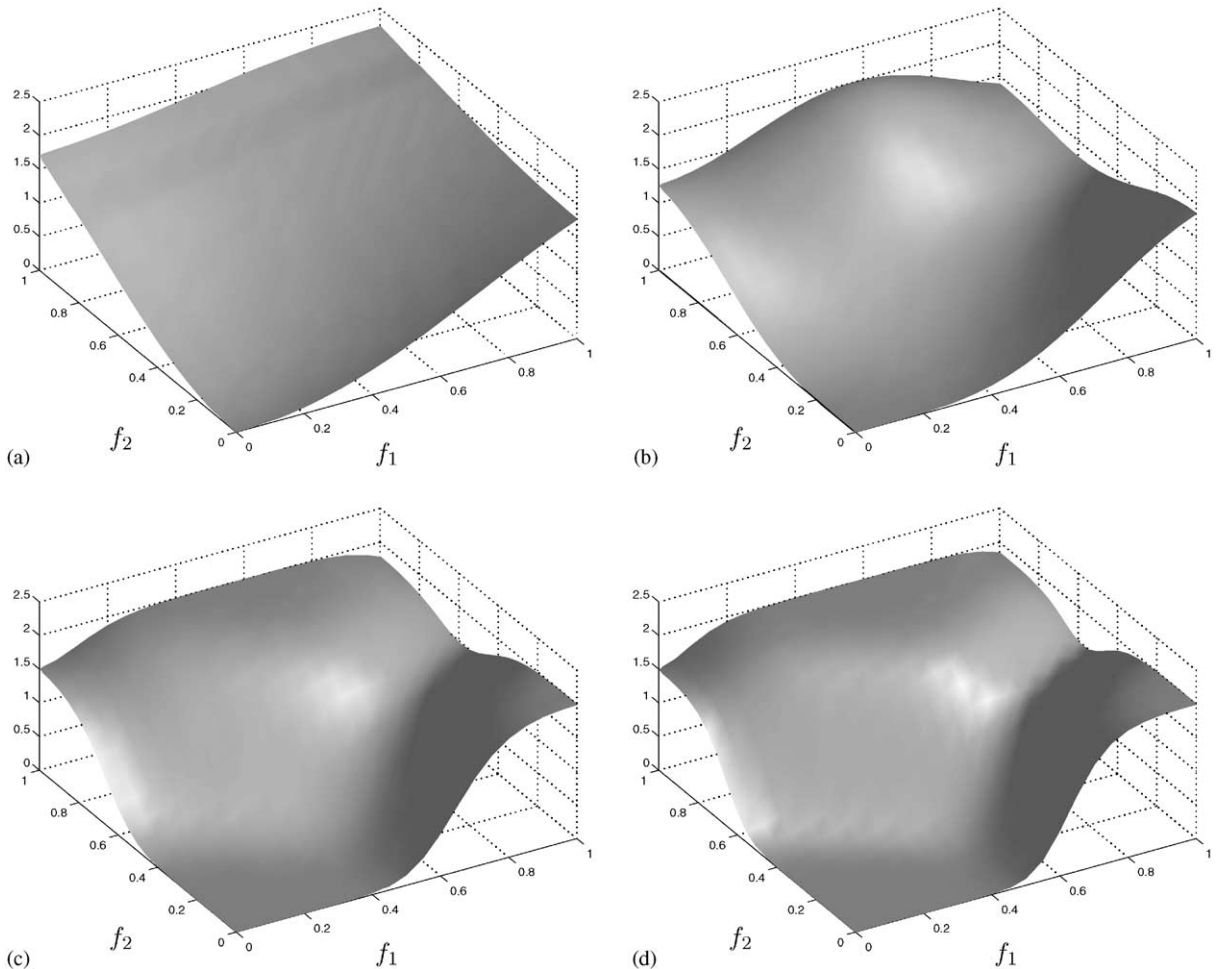


Fig. 15. Interpolation error kernel  $E_{\text{int}}(f)$  for (a) first, (b) second, (c) third and (d) fourth order hexagonal splines.

$m_1 + m_2 \leq L$  are zero. This condition was verified using a software package for symbolic manipulation.

## References

- [1] A. Rosenfeld, A.C. Kak, Digital Picture Processing, 2nd Edition, Academic Press Inc., New York, 1982.
- [2] D. Mitchell, A. Netravali, Reconstruction filters in computer graphics, ACM Comput. Graphics 22 (4) (1988) 221–228.
- [3] J.C. Russ, The Image Processing Handbook, CRC Press Inc., Boca Raton, 1992.
- [4] R. Soinen, Digital Image Resizing Methods, Master's Thesis, Tampere University of Technology, 1994.
- [5] M. Unser, A. Aldroubi, M. Eden, Enlargement or reduction of digital images with minimum loss of information, IEEE Trans. Image Process. 4 (3) (1995) 247–258.
- [6] M. Unser, A. Aldroubi, M. Eden, B-spline signal processing, IEEE Trans. Signal Process. 41 (2) (1993) 821–848.
- [7] C. de Boor, A Practical Guide to Splines, Applied Mathematical Sciences, Vol. 27, Springer, Berlin, 1978.
- [8] H. Hou, H. Andrews, Cubic splines for image interpolation and digital filtering, IEEE Trans. Acoust. Speech Signal Process. 26 (6) (1978) 508–517.
- [9] M. Unser, I. Daubechies, On the approximation power of convolution-based least squares versus interpolation, IEEE Trans. Signal Process. 45 (7) (1997) 1697–1711.

- [10] H. Prautzsch, W. Boehm, in: *Box Splines*, in: *Handbook of Computer Aided Geometric Design*, Springer, Berlin, 2001.
- [11] C. de Boor, K. Höllig, S. Riemenschneider, *Box Splines*, Applied Mathematical Sciences, Vol. 98, Springer, Berlin, 1993.
- [12] C.T. Loop, *Generalized b-spline surfaces of arbitrary topological type*, Ph.D. Thesis, University of Washington, 1992.
- [13] L. Kobbelt,  $\sqrt{3}$ -subdivision, in: *Proceedings SIGGRAPH*, 2000, pp. 103–112.
- [14] G. Nürnberger, F. Zeilfelder, *Developments in bivariate spline interpolation*, *J. Comput. Appl. Math.* 121 (1) (2000) 1–29.
- [15] E. Dubois, *The sampling and reconstruction of time-varying imagery with application in video systems*, *Proc. IEEE* 73 (4) (1985) 502–522.
- [16] R.A. Ulichney, *Digital Halftoning*, MIT Press, Cambridge, MA, 1987.
- [17] M. Unser, *Sampling—50 years after Shannon*, *Proc. IEEE* 88 (4) (2000) 569–587.
- [18] P. Thévenaz, T. Blu, M. Unser, *Interpolation revisited*, *IEEE Trans. Medical Imaging* 19 (7) (2000) 739–758.
- [19] K. Strom, *On convolutions of B-splines*, *J. Comput. Appl. Math.* 55 (1) (1994) 1–29.
- [20] M.-L. Liou, *Spline fit made easy*, *IEEE Trans. Comput.* 25 (1976) 522–527.
- [21] M. Unser, *Fast B-spline transforms for continuous image representation and interpolation*, *IEEE Trans. Pattern Anal. Machine Intell.* 13 (3) (1991) 277–285.
- [22] R.W. Schafer, R.M. Mersereau, M.A. Richards, *Constrained iterative restoration algorithms*, *Proc. IEEE* 69 (4) (1981) 432–450.
- [23] R. Mersereau, *The processing of hexagonally sampled two-dimensional signals*, *Proc. IEEE* 67 (1979) 930–949.
- [24] I. Amidror, *The Theory of the Moiré Phenomenon*, Computational Imaging and Vision, Vol. 15, Kluwer Academic Publishers, Dordrecht, 2000.
- [25] M. Unser, A. Aldroubi, M. Eden, *Polynomial spline signal approximations: Filter design and asymptotic equivalence with Shannon’s sampling theorem*, *IEEE Trans. Inform. Theory* 38 (1) (1992) 95–103.
- [26] D. Petersen, D. Middleton, *Sampling and reconstruction of wave-number-limited functions in N-dimensional Euclidean spaces*, *Inform. and Control* 5 (1962) 279–323.
- [27] T.W. Parks, C.S. Burrus, *Digital Filter Design*, Wiley, New York, 1987.
- [28] T. Blu, M. Unser, *Quantitative Fourier analysis of approximation techniques: Part I—interpolators and projectors*, *IEEE Trans. Signal Process.* 47 (10) (1999) 2783–2795.
- [29] I. Gradshteyn, I. Ryzhik, *Table of Integrals, Series, and Products*, Academic Press, New York, 1994.